Food Biophysics (2021) 16:237–253
https://doi.org/10.1007/s11483-021-09665-z

ORIGINAL ARTICLE

Volume Fraction Measurement of Soft (Dairy) Microgels by Standard Addition and Static Light Scattering

Anisa Heck[1] · Stefan Nöbel[1,2] · Bernd Hitzmann[1] · Jörg Hinrichs[1]

Received: 21 October 2020 / Accepted: 1 January 2021 / Published online: 15 February 2021
© The Author(s) 2021

Abstract

The volume fraction of the dispersed phase in concentrated soft (dairy) microgels, such as fresh cheese, is directly related to structure and rheology. Measurement or modeling of volume fraction for soft and mechanically sensitive microgel dispersions is problematic, since responsiveness and rheological changes upon mechanical input for these systems limits application of typical functional relationships, i.e., using apparent viscosity. In this paper, we propose a method to measure volume fraction for soft (dairy) microgel dispersions by standard addition and volume-weighted particle size distributions obtained by static light scattering. Relative particle volumes are converted to soft particle volume fraction, based on spiked standard particle volumes. Volume fractions for two example microgel dispersions, namely, differently produced fresh cheeses, were evaluated before and after post-treatments of tempering and mechanical processing. By selecting the size of standard particles based on size ratios and the levels of the mixing ratios/relative fractions, the method could be applied robustly within a wide range of particle sizes (1 to 500 μm) and multimodal size distributions (up to quadmodal). Tempering increased the volume fraction for both example microgel dispersions ($P < 0.05$). Subsequent mechanical treatment reduced the volume fraction back to the starting value before tempering ($P < 0.05$). Furthermore, it was shown that the increase and successive decrease in apparent viscosity with tempering and mechanical post-treatments is not exclusively due to particle aggregation and breakdown, but to volume changes of each particle. For environmentally responsive soft matter, the proposed method is promising for measurement of volume fraction.

Keywords Fermented milk · Biopolymer · Thermoquark · Phase volume · Volume concentration · Laser diffraction

Introduction

Microgels are dispersions of soft particles with a large volume of solvent within their structure. This type of dispersion is widespread in nature and industry, for example oil and drilling, mineral processing, personal care products and foods [1]. Different polymer makeup, production methods and post-production processing of microgel dispersions result in particles of varying characteristics, such as size, firmness, elasticity, surface charge, and solvent binding capacity [2]. Due to the nature of the polymer network that forms the microgel particles, swelling or compression can occur from changes in environmental conditions, i.e., mechanical input, physiochemical changes, and temperature, which results in fluctuations in the amount of solvent within the particles. Since the volume occupied by each microgel particle is highly dependent on these factors, the volume fraction ϕ (*v*/v) of the dispersed phase is not well defined and is difficult to measure [1, 3]. As a result, the flow behavior of microgel dispersions is highly complex. Fundamental knowledge of the relationship between microgel (micro- and macro-)structure and rheology is limited to dispersions of microgel particles synthesized with a defined polymer makeup and microstructure [1, 4–8]. As the complexity of the microgel particle makeup and microstructure increases, for example for bio-polymer and food microgel particles, structure – function relationships are increasingly difficult to define [2].

Fermented dairy products, such as yogurt and fresh cheese, can be classified as dispersions of microgel particles [9, 10]. As with typical microgel particles, characteristics of fermented dairy microgel particles are modified during production and post-processing steps, such as tempering and mechanical

✉ Anisa Heck
anisa.heck@uni-hohenheim.de

[1] University of Hohenheim, Institute of Food Science and Biotechnology, D-70593 Stuttgart, Germany

[2] Present address: Max Rubner-Institut, Department of Safety and Quality of Milk and Fish Products, D-24103 Kiel, Germany

treatment [9, 11, 12]. Consequently, physical properties of these semi-solid dairy products, such as apparent viscosity and particle size, are affected; these parameters are key during processing, in terms of unit operations, i.e., pumping, heat transfer, and mixing. These physical properties are also important for consumer acceptance, because they define mouthfeel, optical appearance and product stability [13]. Therefore, knowledge of volume fraction, along with rheological and particle characteristics, is essential in understanding and being able to tailor the textural properties of fermented dairy microgel dispersions, based on process modifications.

Volume fraction ϕ (mL_{par}/mL_{total}) is relatively easy to define for "hard" (non-deformable, non-interacting) spheres solely drawing on density and mass. An additional format of this equation can be applied for dilute microgel dispersions, which takes into account the specific volume of the dispersed substance k (mL_{par}/g_{par}) and mass concentration of solid β (g_{par}/mL_{total}), or in another form, the apparent voluminosity υ_{app} (mL_{par}/g_{par}) of microgel particles, the dispersion density ρ (g_{total}/mL_{total}), and mass concentration w (g_{par}/g_{total}).

$$\phi_{\mathrm{eff}} = k \cdot \beta = \upsilon_{\mathrm{app}} \cdot \rho \cdot w \tag{1}$$

The difficulty in applying this equation lies in accurate measurement of k or υ_{app}, respectively, since the specific volume is not constant and relates to the fluctuating amount of solvent entrapped within the polymer matrix of microgel particles. These parameters can be evaluated, for example, by rheometry [14, 15] or centrifugation [16]. Nevertheless, both these methods have a major drawback of highly affecting the state of the sample and, hence, the volume fraction, i.e., through mechanical input.

For dispersions of soft microgel particles, the concept of volume fraction is complex and may not be constant with increases in concentration. In the dilute regime ($\phi < 0.01$), microgel dispersions follow hard particle suspension rheology; thus, Einstein's viscosity equation can be used to estimate the effective volume fraction ϕ_{eff}, by assuming that it is equal to the absolute volume fraction ϕ,

$$\eta_{\mathrm{r}} = \frac{\eta_{\mathrm{d}}}{\eta_{\mathrm{c}}} = 1 + 2.5\phi \tag{2}$$

where η_{r} is the relative viscosity (−) given as the viscosity ratio of the discontinuous phase, i.e., dispersed phase, η_{d} (Pa s) to the continuous phase, i.e., dispersion medium, η_c (Pa s), and 2.5 stands for a spherical particle in a shear flow [2]. With increasing volume fraction ($\phi > 0.2$), microgel particles come into close contact, causing other interactions that need to be taken into account. These other interactions are included in the Krieger-Dougherty equation, where the volume fraction ϕ of the dispersed phase in concentrated dairy microgel dispersions ($\phi \geq 0.4$) is described,

$$\eta_d = \eta_{\mathrm{c}} \left(1 - \frac{\phi}{\phi_{\max}}\right)^{-[\eta]\cdot\phi_{\max}} \tag{3}$$

where $[\eta]$ is the intrinsic viscosity (−), ϕ is the hydrodynamic volume fraction (−), and $\phi_{\max}$ is the maximum packing fraction (−). An alternative equation relevant for $0.3 < \phi < 0.5$, which reduces the number of unknown variables, is referred to as the MPQ model [14, 17–19].

$$\eta_d = \eta_{\mathrm{c}} \left(1 - \frac{\phi}{\phi_{\max}}\right)^{-2} \tag{4}$$

For mono- and polydispersed hard- spheres, $\phi_{\max}$ can be reasonably predicted by the packing fraction of randomly close packed spheres ϕ_{rcp} and substituted into the model [13, 17, 20]. With increasing volume fraction, as well as decreasing particle modulus and cross-linking density, the exact value of $\phi_{\max}$ becomes more dominant [1, 14]. The so-called "crowding effect" occurs, where close packing of particles impedes rotation and causes deformation or even destruction of microgel particles, leading to changes of both ϕ and $\phi_{\max}$ [2, 21]. Thus, for soft microgel dispersions with variable υ_{app}, this substitution is not valid and leads to deviations from the models, particularly as $\phi \rightarrow \phi_{\max}$ [1]. The complexity of defining ϕ of microgel dispersions is further escalated, given that the apparent viscosity η' of microgel dispersions is a function of additional factors, for example shear stress σ, shear rate $\dot{\gamma}$, temperature ϑ, and time t [2, 12]. Therefore, estimating the volume fraction for soft and mechanically sensitive microgel dispersions is challenging, since these typical functional relationships (Eqs. 2–4) or mechanical separation cannot be applied.

This study presents a step-by-step procedure to analyze the volume fraction of environmentally responsive microgel dispersions and soft matter systems by standard addition (PMMA particles) and analysis of volume distributed particle size using static light scattering. The requirements for standard particle selection and conditions for particle size analysis, based on mixtures with microgel particles, are reviewed and optimized. The method is applied to fresh cheese, an example of a fermented dairy microgel dispersion, as a complex model system with sensitivity to environmental changes, including thermal and mechanical input.

Materials and Methods

Production of Example Microgel Dispersions

Fresh cheeses (process variants A and B) were produced using pasteurized milk (<0.1%, *w*/w fat; 74 °C for 30 s) as described by Hahn et al. [9] with the following modifications. Fermentation to a pH of 4.45 to 4.50 was carried out at 22.5 °C by suspending 0.04% (w/w) CHOOZIT 230

(Danisco, Niebüll, Germany) mesophilic starter culture containing *Lactococcus lactis* subsp. *lactis* and *Lactococcus lactis* subsp. *cremoris* and adding 1 mL/100 L rennet (ChyMax Plus; Chr. Hansen GmbH, Nienburg, Germany; min. 190 IMCU/mL). Following fermentation, the gel for process variant B was pre-heated in a tubular plant (150 L/h, ASEPTO-Therm; Asepto GmbH, Dinkelscherben, Germany) to 64 °C for 4.3 min and cooled to 38 °C; this step was omitted for process variant A. After filtration (38 °C, nominal pore size 0.06 μm), both process variants were cooled to ≤14 °C (ΔT = 24 K in <10 s) by pumping through a screw pump (Nemo nM021; Netzsch Mohnopumpen GmbH, Waldkraiburg, Germany) at 250–255 L/h connected to a double walled heat exchanger cooled with ice water (length 1.86 m, active area 0.4 m^2). Process variant A was filled into 5 L steel canisters; process variant B was filled into 100 mL cylindrical glasses. Samples were stored overnight (20 to 22 h) at 6 °C. Post-treatment for process variant A was conducted by (batch) tempering in the steel canisters in a water bath at 38 °C for 300 min followed by 18 h of storage at 6 °C. Four canisters of the tempered process variant A were filled into a feed funnel connected to a pump (Nemo nM021), and mixed up and down ten times by hand using a steel perforated plate stirrer. The tempered and mixed process variant A was pumped at 250 to 255 L/h through a rotor – stator system (Ytron: Z 1.50(FC)-2.0.1; Ytron Process Technology GmbH & Co KG, Bad Endorf, Germany) set at 0, 1800 and 4500 1/min and then filled into 100 mL cylindrical glasses. Samples were stored at 6 °C for a minimum of 18 h until further analysis. Glass jars filled with process variant B were tempered in a water bath at 38 or 45 °C for 300 min, followed by a minimum of 18 h of storage at 6 °C until further analysis. Each process variation was produced once and the subsequent post-treatment variants were prepared using the single process variant production.

Particle Size Measurement

The volume-weighted particle size distributions of all samples were analyzed using static laser light scattering (Beckman Coulter LS 13320 fitted with a Universal Liquid Module and control software v6.01, Beckman Coulter Inc., Miami, FL, USA). The instrument was set to split the measurement range of 0.04 to 2000 μm into 116 channels based on a logarithmic scale, where each channel represents one possible data point. For every measurement, three consecutive runs of 60 s each were conducted at a maximum obscuration and PIDS of 15 and 50%, respectively. An average of the three runs was automatically calculated by the instrument software. A minimum of either 5% obscuration or 10% PIDS was obeyed for each measurement. To reach these minimum values, 0.2 to 2 mL of sample was added to the measurement chamber. The pump speed was 51% of the maximal value. A real refractive index of 1.57 was determined for the microgel particles in the example microgel dispersions using the method described by Hayakawa et al. [22]. Though the manufacturer's specification indicates a real refractive index of 1.487 to 1.492 for the standard particles, a range of 1.49 to 1.58 was deemed acceptable following the same method by Hayakawa et al. [22]. Therefore, a real refractive index of 1.57 for particles was selected for mixtures of standard particles, as well as for mixtures of standard particles and the example microgel particles. The real refractive index of the solvent (water) was 1.33 [23]. The imaginary refractive indices for particles and water were set at 0.00, since the materials were white or transparent [24]. The particle size distributions for each standard particle and process variant (A and B) with subsequent post-treatments were measured a minimum of three times and the volume-based average equivalent diameter $d_{50,3}$ was calculated. Span, defined as the difference between $d_{10,3}$ and $d_{90,3}$, was also calculated and given as a range (minimum and maximum values).

Density

Density was evaluated using a densitometer (DMA5000; Anton Paar, Graz, Austria) at 20 °C. The density of each standard particle was determined individually. To calculate the standard particle density ρ_{sp} from Eq. 5, 4 to 6 g of standard particle m_{sp} were mixed with 15 to 20 g silicon oil m_{so} (M 1000, $v = 1000$ mm^2/s; Carl Roth GmbH, Karlsruhe, Germany) and total density ρ_{total} was measured.

$$\rho_{\text{total}} = \left(m_{sp} + m_{\text{so}}\right) / \left(\frac{m_{\text{sp}}}{\rho_{\text{sp}}} + \frac{m_{\text{so}}}{\rho_{\text{so}}}\right) \tag{5}$$

Standard particle density ρ_{sp} was used to calculate the standard particle specific volume k. Mixtures for each standard particle were prepared at a minimum in triplicate. The densities of pure silicon oil (ρ_{so}=0.973 ± 0.001 g/mL), process variants A and B were also evaluated. Density was measured a minimum of 15 times for each sample.

Standard Addition

Uncoated spherical poly(methyl methylacrylate) (PMMA) particles (CA15, CA30, CA40, CA60; Microbeads AS, Skedsmokorset, Norway) with nominal sizes ($d_{4,3}$) of 15, 30, 40, and 60 μm (coefficient of variation = 5%), respectively, (manufacturer's specification), were selected relative to the example microgel particles' size range (1 to 500 μm). For method validation, bi-, tri- and quadmodal mixture designs for all possible combinations of standard particles (bimodal: CA15–CA30, CA15–CA40, CA15–CA60, CA30–CA40, CA30–CA60, CA40–CA60; trimodal: CA15–CA30–CA40, CA15–CA40–CA60, CA30–CA40–CA60; quadmodal:

CA15–CA30–CA40–CA60) were defined using a simplex lattice mixture design and a lattice degree of three (Minitab v17.2.1; Minitab Inc., State College, PA, USA). To define the sample compositions to be prepared (standard particle mixtures dispersed in distilled water), minimum and maximum standard particle relative volumes were set at 10 and 90%, respectively, with a total constant standard particle volume of 100%. Within the mixture designs, each design point, i.e., sample composition, was replicated, for a total of 14, 26, and 50 points in bi-, tri- and quadmodal mixture designs, respectively. The preparation of design points in each mixture design was as follows: For each mixture design, 2.0% *v*/v standard particle dispersions were prepared in distilled water, based on the standard particle specific volume k ($k_{CA15} = 0.847$, $k_{CA30,\ CA40,\ CA60} = 0.852$) determined from density measurements ("Density" section). For each design point, aliquots of the standard particles in the mixture design, e.g., CA15 and CA30 in the CA15–CA30 bimodal mixture design, were pipetted into a 5 mL centrifuge tube at relative standard particle volumes defined by the design point. The centrifuge tube was inverted 10 times to mix, and the particle size distribution was evaluated directly.

To analyze the volume fraction of the example microgel dispersions, 1 to 3 g of a given type of standard particle or 3 to 5 g of a given example microgel dispersion were diluted in 48 to 52 g distilled water and stirred for 15 min at 450 1/min. Distilled water was chosen as the medium in which to dilute the example microgel dispersions and evaluate the particle size distributions, since no significant difference in particle size was found when fat-free fermented concentrated dairy microgel dispersions were diluted and evaluated in distilled water compared to the native dispersion medium, i.e., permeate obtained during the concentration (microfiltration) of the fermented concentrated dairy microgel particles [9]. Furthermore, distilled water has a known refractive index and this information is required of the dispersion medium used during static light scattering measurements. Masses were recorded and particle size distributions were analyzed. An aliquot of the diluted example microgel dispersion was then spiked with the standard particle dispersion and the particle size distribution was subsequently evaluated. A minimum of five spiking concentrations were measured in combination with aliquots from each diluted example microgel dispersion. For each different example microgel dispersion (process variants A and B) and the different post-treatment variations, a minimum of six individual samples were diluted and analyzed.

Peak Fitting and Calibration

Bi-logarithmic plots of volume-weighted particle size distributions were fitted to Gaussian peaks (≤7) by Least Squares Regression analysis, using the add-in Solver tool in MS Excel (Microsoft Office 2013; Microsoft Corporation, Redmond, WA, USA) and a spreadsheet adapted from Tom O'Haver (https://terpconnect.umd.edu/~toh/spectrum/CurveFittingC.html#Spreadsheets). The (analyzed) estimated relative volumes of standard particle to standard particle, or standard particle to microgel particle, were based on the area of peak(s) attributed to the specific particle, out of the total peak area. These steps can be reproduced in an example spreadsheet for a quadmodal mixture of standard particles (Electronic Supplementary Information). Relative peak area represents relative particle volume, as particle size distributions are volume weighted. A calibration curve for microgel particle volume was constructed for each set of spiked microgel dispersion samples and used to calculate the microgel dispersion volume fraction ϕ_{mgp}. The standard particle relative volume, rel. ϕ_{sp}, over the microgel particle relative volume, rel. ϕ_{mgp}, for each spiked sample was plotted against the standard particle volume concentration ϕ_{sp} (in mL/mL of undiluted microgel dispersion) in the respective sample mixture. Regression analysis was used to calculate the standard particle volume concentration for the relative peak ratio of 1:1, which represents the (microgel) particle volume per mL of microgel dispersion (Eq. 6).

$$\phi_{calc} = \phi_{sp} = \lim_{\text{ratio}\to 1:1} \text{rel.}\phi_{sp}/\text{rel.}\phi_{mgp} \tag{6}$$

For each standard particle–microgel dispersion mixture type, six calibration curves were prepared.

Rheological Characterization

Flow curves were collected using a stress-controlled rheometer AR 2000 (minimum torque: 9.1 nNm; TA Instruments Inc., Eschborn, Germany) with a concentric cylinder cup and bob system (stator inner radius: 15.0 mm, rotor outer radius: 14.0 mm) according to Körzendörfer et al. [10]. Before the measurement, each sample was briefly stirred with a plastic spoon. Between 16 and 17 g of the sample was transferred into the cup. The sample was cooled to 10 °C and equilibrated for 15 min. The shear rate was linearly increased from 0 to 500 1/s within 3 min, followed by a hold step at 500 1/s for 3 min. Finally, the shear rate was decreased to 0 1/s within 3 min in a linear fashion to result in a flow curve. Measurements were performed in duplicate at 10 °C. The viscosity at a shear rate $\dot{\gamma}$ of 100 1/s was calculated.

Protein Analysis

The protein content was analyzed based on the method of Dumas (IDF 185) using a nitrogen analyzer (Dumatherm DT; C. Gerhardt GmbH & Co. KG, Königswinter, Germany). The protein contents of process variants A and B were calculated by multiplying the total nitrogen content with a conversion factor of 6.38. Each sample was measured at a minimum in triplicate.

Statistical Analysis

The divergence between the given and estimated relative volume (% residual error) for bimodal mixture design points was evaluated by regression analysis of each bimodal mixture design, using backward model selection (Minitab v17.2.1). Models were selected from linear, quadratic and inverse terms, based on $\alpha \leq 0.10$. Pearson correlation coefficients were calculated to investigate the relationships between (absolute) residual error (%), number of channels per peak (data points), peak location (in μm), peak width (in μm), peak fitting error (%), total overlap of peaks (%), overlap of individual peak (%), and size ratio of particles (larger particle [center of fitted peak in μm] / smaller particle [center of fitted peak in μm]) (Sigmaplot v12.5; Systat Software, Inc., San Jose, CA, USA). Correlations were calculated for data from individual bimodal mixture designs, as well as the sum of all data from all bimodal mixture designs.

For statistical analysis of the density, particle size, volume fraction and rheological parameters, the arithmetic mean values and standard deviations were calculated and are given in the text. Significant differences were analyzed in Sigmaplot by ANOVA and Tukey's post-hoc test using $\alpha = 0.05$.

Results and Discussion

Based on the principles of static light scattering, the standard particles used to calculate the volume of unknown microgel particles should be 1) spherical, 2) inert and 3) within the size range of analysis. Particles should also be easy to obtain and low cost. In addition, standard particles should be low density (<2 g/cm^3), in order to prevent sedimentation during the measurement, which is dependent on the set pump speed. Further requirements for standard particles also depend on the characteristics of the microgel particles in question. Since the particle size distributions of standard and targeted (microgel) particles are determined simultaneously, standard particles should have a similar refractive index to the microgel particles (real refractive index = 1.57, determined for the example microgel particles). Additionally, the standard particles should not be the same size as the microgel particles, so that the standard particles can be differentiated when observed within the analyzed particle size distribution (peak overlap). To ensure that a variety of microgel particle sizes can be analyzed, it is essential to have a range of standard particles of different sizes. The volume-based average equivalent diameters ($d_{50,3}$) of the spherical PMMA particles, namely, CA15, CA30, CA40 and CA60 were 13.7 ± 0.1, 28.8 ± 0.1, 41.5 ± 0.1, and 56.6 ± 0.1 μm ($n = 3$). Furthermore, all size distributions were monomodal. These characteristics, along with densities of <2 g/cm^3 and an optimized real refractive index range for measurements with the LS 13320 of 1.49 to 1.58, make these particles suitable as standard particles to calculate the volume fractions of the example microgel dispersions in this study.

Method Development

Within the mixture designs of two, three and four standard particles, samples having different given relative volumes (out of 100%) and bi-, tri- and quadmodal particle size distributions were analyzed by static light scattering. The quality of the prediction of standard particle relative volume from different mixing ratios was evaluated on the basis of the residual error (Fig. 1; Appendix: Figs. 5 and 6), by comparing the estimated relative volume with the given relative volume, as calculated from the initial sample weight ($\beta = 0.01$ to 0.05 g/mL) and the standard particle specific volume k ($k_{CA15} = 0.847$, $k_{CA30,\ CA40,\ CA60} = 0.852$) according to Eq. 1. Estimated relative volumes were calculated from the fitted particle size distributions, where the peak volume for each standard particle is given out of 100%. Ideally, all measurement points for residual error would lie on the horizontal line, which represents residual error of zero (Fig. 1; Appendix: Figs. 5 and 6). The factors affecting data precision and accuracy, meaning the measure of the quality and repeatability of the measurements and automatic evaluations, and the prediction of the actual relative volumes from the real measured data, respectively, are discussed in the "Factors contributing to residual error" section.

For bimodal mixture designs of standard particles CA15–CA30, CA15–CA40, CA15–CA60 and CA30–CA60, the residual errors are between −5 and + 5%, whereas for bimodal mixture designs of CA30–CA40 and CA40–CA60 they are between −10 and + 10% (Fig. 1). However, it should be noted that in the CA40–CA60 mixture design, the residual errors are between +5% and − 5% for relative volumes of >10% and <90%. In these cases, the peaks for the standard particles with a relative volume of <10% did not appear in the analyzed particle size distributions. A tendency for higher residual error is shown for bimodal mixture designs with a lower size ratio between particles, i.e., the centers of the two peaks in the particle size distribution are closer together. This tendency is also clear when comparing the residual errors from trimodal mixture designs of CA15–CA30–CA60 and CA15–CA40–CA60 (Appendix: Fig. 5). The residual errors from the CA15–CA40–CA60 mixture design range from −14 to +10%. However, in the CA15–CA30–CA60 mixture design, residual errors do not occur lower or higher than −5 and + 5%, respectively. This aligns with what is shown for bimodal standard particle mixture designs, where residual error is higher for combinations of standard particles where peaks are located closer together in the particle size distribution, i.e., smaller size ratios. Residual errors for the quadmodal mixture design are similar to the trimodal mixture design of CA15–CA30–CA60, ranging between −13 and + 10% (Appendix: Fig. 6). Though there appears to be a relationship between the given relative volume and residual error for

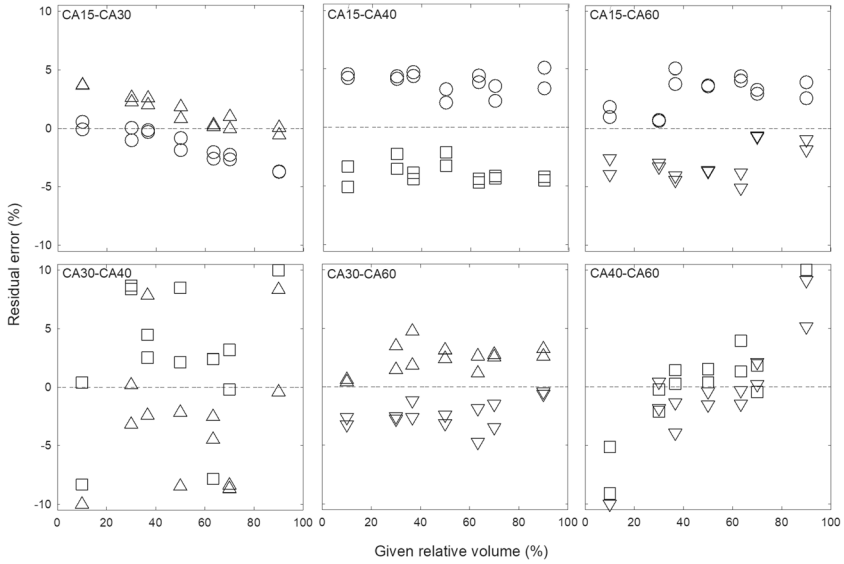

Fig. 1 Residual error of the fitted particle size distributions in relation to sample composition of bimodal standard particle mixtures in terms of standard particle relative volume (CA15 ○; CA30 Δ; CA40 □; CA60 ▽); error is defined as over or under assessment of relative particle volume in comparison to sample composition (given relative particle volume); dotted line indicates 0% error

some standard particle bimodal, i.e., CA15–CA30, CA30–CA40 and CA40–CA60 (Fig. 1), and trimodal mixture designs, i.e., CA15–CA30–CA60 (Appendix: Fig. 5), no clear conclusion can be drawn from these figures; residual error is inferred to be multifactorial and is discussed in the following section.

Factors Contributing to Residual Error

Residual error may be the product of three main contributing groups of factors, some of which interact with each other: 1) compositional factors, 2) analysis factors and 3) computational factors. Compositional factors include the given relative volume of particles, the size ratio, overlap of peaks, and width of the peaks (related to peak shape and size). Analysis factors, on the other hand, are those that cannot be directly affected by external and metrological factors; these are built into the method of analysis. The number of channels allotted to each particle in the distribution (data points per peak) and measured particle size (peak location) are related to the equipment used for analysis. The main computational factor occurs when fitting the distribution into individual peaks. Additionally, the selection of the materials' refractive indices (real and imaginary) fall into this category. All three contributions are analyzed in detail for bimodal standard particle mixture designs, whereby the Pearson correlation coefficients between quantitative factors are displayed in Table 1.

Compositional Factors

Regression analysis of bimodal mixture designs in terms of the relationship between the given relative particle volume and residual error give an indication of how residual error is related to the sample composition. For bimodal mixture designs of CA15–CA30, CA15–CA40, CA30–CA60 and CA40–CA60, the residual errors were fit successfully to models (Appendix: Table 4). For both CA15–CA30 and CA15–CA40 mixture designs, only the linear terms were significant. Only the inverse term for CA30 was significant for the mixture design of CA30–CA60. For the CA40–CA60 mixture design, the quadratic and inverse terms for CA60 were significant. Though there are significant relationships between residual error and the given relative particle volume for these bimodal mixture designs, different significant terms indicate that the relationship is not constant for all mixtures; this suggests involvement of further factors that drive residual error. There is a weak correlation between residual error and the given standard particle relative volume ($r = 0.23$, $P < 0.01$), when the data from all design points in all bimodal standard particle mixture designs are combined, which is in line with observations from individual bimodal mixture designs. For further comparison, the residual error was converted to absolute residual error. This conversion was done to focus on accumulated error; where absolute residual error, the distance from zero, is in focus, rather than the distance plus direction, i.e., positive or negative. The resulting correlation between the given standard particle relative volume and absolute residual error is not significant ($P > 0.1$, Table 1).

The next compositional factor of interest is the size ratio. The size ratios for bimodal standard particle mixture designs, in ascending order, are 1.24 ± 0.05, 1.41 ± 0.02, 2.11 ± 0.09, 2.17 ± 0.04, 3.10 ± 0.12, and 4.46 ± 0.15 for CA30–CA40, CA40–CA60, CA30–CA60, CA15–CA30, CA15–CA40, and CA15–CA60, respectively (Table 2). There is a very weak negative correlation between absolute residual error and size ratio ($r = -0.16$, $P \leq 0.05$) (Table 1). From this, it is deduced that clear peak separation may reduce the absolute residual error.

Since correlations between residual error and size ratio for all design points from all bimodal standard particle mixture designs (Table 1) and design points in the individual bimodal

Table 1 Pearson correlations between quantitative measurement parameters for the volume analysis of spherical PMMA particles in bimodal mixtures by static light scattering (LS 13320)

	Composition					Analysis		Computation
	Pairwise			Individual				
	Given relative volume	Size ratio	Total overlap	Individual peak overlap	Peak width	Channels per peak	Peak location	Fitting error
Size ratio	<0.001							
Total overlap	<0.001	-0.47***						
Individual peak overlap	-0.17*	-0.41***	0.77***					
Peak width	0.27***	-0.19**	0.19*	0.07				
Channels per peak	0.37***	0.09	0.09	-0.06	0.42***			
Peak location	0.12	-0.08	0.09	0.08	0.74***	-0.14•		
Fitting error	-0.36***	-0.08	0.04	0.50***	-0.14•	-0.30***	0.09	
Absolute residual error	<0.001	-0.16*	0.09	0.11	-0.13	-0.15*	-0.11	0.15•

Correlations are calculated using the collective results from all design points in all bimodal standard particle mixture designs (pairwise: n = 84; individual: n = 168)

•, *, **, *** Significant differences: $P \leq 0.1$, $P \leq 0.05$, $P \leq 0.01$, $P \leq 0.001$

Table 2 Compositional, analysis and computational measurement parameters (arithmetic mean ± standard deviation, $n = 14$) and their Pearson correlation coefficients (r) with absolute residual error of the volume analysis from bimodal mixtures of spherical PMMA particles analyzed by static light scattering (each parameter tested individually against absolute residual error)

	Composition								Analysis				Computation	
	Pairwise				Individual									
	Size ratio (−)	r	Total overlap (%)	r	Overlap of peak (%)	r	Peak width (μm)	r	Number of channels (−)	r	Peak location (μm)	r	Fitting error (%)	r
CA15-CA30	2.17±0.04	−0.93***	*NA*	*NA*										
CA15					*NA*	*NA*	4.8±1.0	0.89***	7.1±1.6	0.86***	12.6±0.2	0.93***	1.4±1.4	−0.65**
CA30					*NA*	*NA*	10.2±1.0	−0.73**	7.2±0.8	−0.52•	27.3±0.2	−0.64**	1.0±0.6	0.65**
CA15-CA40	3.10±0.12	0.43	*NA*	*NA*										
CA15					*NA*	*NA*	6.7±2.0	0.50•	9.8±2.9	0.48•	12.5±0.4	−0.54*	1.8±2.4	0.32
CA40					*NA*	*NA*	14.3±5.0	0.36	6.9±2.7	0.38	38.8±0.7	0.02	1.7±2.1	0.38
CA15-CA60	4.46±0.15	0.17	*NA*	*NA*										
CA15					*NA*	*NA*	6.5±1.3	−0.48•	9.3±1.6	−0.37	12.8±0.3	−0.04	2.1±1.8	−0.25
CA60					*NA*	*NA*	15.8±7.4	−0.47•	5.3±2.5	−0.54*	57.2±1.6	0.20	2.1±2.4	0.24
CA30-CA40	1.24±0.05	0.53•	10.2±4.2	−0.59*										
CA30					24.3±17.1	−0.56*	11.9±1.5	−0.50•	7.8±1.0	−0.44	29.3±1.4	−0.56*	2.3±2.1	−0.61*
CA40					29.2±17.7	−0.24	14.4±4.6	0.01	7.3±2.4	0.12	36.7±1.4	0.32	6.2±14.2	0.12
CA30-CA60	2.11±0.09	−0.60*	0.1±0.4	0.46•										
CA30					0.3±0.1	0.42	11.8±3.8	0.58*	8.0±2.5	0.67***	26.6±1.1	0.61*	1.1±0.6	−0.53*
CA60					0.2±0.1	0.47•	20.1±9.2	0.04	6.9±2.9	0.01	56.1±0.4	−0.13	1.7±2.2	0.30
CA40-CA60	1.41±0.02	−0.75**	2.4±1.4	−0.76**										
CA40					5.7±2.1	−0.72**	14.4±3.6	−0.41	6.6±1.9	−0.42	40.2±0.5	−0.6*	4.2±8.6	0.46•
CA60					5.8±5.0	−0.53*	24.7±6.3	−0.70**	8.3±1.8	−0.68**	56.7±0.6	−0.77	2.8±4.2	−0.35

NA Not applicable (no overlap of peaks)

•, *, **, *** Significant differences noted $P \leq 0.1$, $P \leq 0.05$, $P \leq 0.01$, $P \leq 0.001$

mixture designs (Table 2) do not give information regarding a potential size ratio threshold for minimizing residual error, the fit of regression models relating given relative volume to residual error is discussed, using the standard error of the estimate (SER) (Appendix: Table 4). For models that have no constant (mixture designs), SERs are used to describe how well a model fits the data. The unit of SER is the same as the response variable (residual error, %) and represents how far the results of the response variable fall from the fitted values of the regression. SERs of the fitted models are related to size ratios in the following manner: Mixtures with size ratios ≥1.41 (CA15–CA40, CA15–CA30, CA15–CA60, CA30–CA60, and CA40–CA60) have a SER of ≤1.5% (and no lack of fit), indicating that the residual error values lie on average ≤1.5% higher or lower than the calculated (successfully fitted) regression model values (Appendix: Table 4). However, the mixture with a size ratio of 4.46 (CA15–CA60) was not fit successfully to a model (failed lack of fit testing). Furthermore, the mixture with a size ratio <1.41 (CA30–CA40) has a SER of 4.2, indicating that the residual error values lie on average 4.2% higher or lower than the fitted model values (Appendix: Table 4). Consequently, residual errors are the lowest for mixtures with size ratios ≥1.41 and <4.46 (Table 1).

When the ratio between the sizes of particles is smaller, the probability is higher that the two peaks overlap in the distribution. Therefore, residual error could be a result of a small size ratio, overlap of the peaks, or a combination of both. Two statistics were calculated to characterize the overlap of peaks in the particle size distribution: total and individual peak overlap. Total peak overlap is the proportion of the total peak volume that is overlapped within the whole distribution (% of total peaks), whereas individual peak overlap is the volume of an individual peak that is located in an overlapping region (% of individual peak). Total peak overlap and individual peak overlap are not significantly correlated with absolute residual error (Table 1); however, both are moderately (negatively) correlated with the size ratio (total peak overlap: $r = -0.47$, $P \leq 0.001$; individual peak overlap: $r = -0.41$, $P \leq 0.001$). This finding was anticipated, given that peaks that are far away from each other cannot overlap. Since peak overlap is observed in some, but not all, of the bimodal mixture designs, a closer look at those with overlap is warranted. Peak overlap is measurable for design points in bimodal mixture designs of CA30–CA40, CA30–CA60 and CA40–CA60 (Table 2). Of the three bimodal mixture designs with overlap, one bimodal combination, namely, CA30–CA60, has minimal total and individual peak overlap (<0.5%, Table 2). The total overlap for design points in CA30–CA40 and CA40–CA60 bimodal mixture designs is 10.2 ± 4.2 and 2.4 ± 1.4%, respectively, and individual peak overlap for each standard particle is 2–3 times higher than total overlap for both bimodal designs. Moderate to strong (negative) correlations between total peak overlap and absolute residual error for these two bimodal mixture designs (CA30–CA40: $r = -0.59$, $P \leq 0.05$; CA40–CA60: $r = -0.76$, $P \leq 0.01$) provide evidence that these factors are related; however, only at low size ratios (<1.41), where overlapping is dominant (Table 2). Since the amount of overlap for these combinations of standard particles also decreases with increasing size ratio, it is possible that a cause and effect relationship is present, whereby small size ratios result in peaks that are close together, increasing the likelihood of peak overlap and, thus, resulting in insufficient fitting.

Significant positive or negative correlations are found between absolute residual error and peak width (in μm) for at least one individual standard particle in each bimodal mixture design; however, moderate to strong correlations with $P \leq 0.05$ are found only for CA15 ($r = 0.89$, $P \leq 0.001$) and CA30 ($r = -0.73$, $P \leq 0.01$) in the CA15–CA30 mixture design, CA30 ($r = 0.58$, $P \leq 0.05$) in the CA30–CA60 mixture design and CA60 ($r = -0.70$, $P \leq 0.01$) in the CA40–CA60 mixture design (Table 2). Furthermore, when the data is compiled from all bimodal mixtures, no significant correlation between peak width and absolute residual error remains (Table 1).

Analysis Factors

Due to the logarithmic spacing of the particle size distribution using laser scattering devices, like the LS 13320, there is a risk that peaks have a different number of data points, depending on peak location and width, i.e., (detection) channels. Though some significant correlations are identified for individual particles in the bimodal mixture designs (Table 2), the overall correlation of absolute residual error with number of channels per peak for all mixture designs combined, provides a better view of the complete relationship (Table 1). Absolute residual error is very weakly correlated with a decreasing number of channels per peak ($r = -0.15$, $P \leq 0.05$), in contrast to peak width, where no significant correlation is found ($P > 0.10$). This indicates that error is less related to the actual width (μm) of the peak, and more related to the ability of the equipment to collect data points within a specific size range (spatial resolution). The following correlations relate the sample composition to the number of channels per peak: peak width and the given relative volume are (weakly to moderately) positively correlated with the number of channels per peak (peak width: $r = 0.42$, $P \leq 0.001$; given relative volume: $r = 0.37$, $P \leq 0.001$, Table 1). In other words, as the given relative volume and peak width increase, the number of channels per peak increases, which leads to a reduction in absolute residual error. This corroborates the limited sensitivity when the given relative volume is ≤10 or ≥90%.

If a single particle is analyzed multiple times using the same equipment, the resulting values are expected to be within a certain random range (within-subject variability). In spite of this, there are deviations in the mean particle size values, depending on whether a mixture of particles (collective) or a single particle is measured, due to matrix effects, i.e., shifts

in the refractive index and scattering patterns. Thus, a shift in peak location is accompanied by a shift in the volume ratio between peaks, which negatively affects the accuracy of the volume fraction calculation based on this volume ratio. Since the correlation between peak location and absolute residual error is not significant (Table 1), a significant influence of this parameter on the calculated volume fraction is not anticipated.

Computational Factors

When a multimodal volume-weighted particle size distribution is obtained using static light scattering, additional computational effort is required when peak superposition occurs. The volumes of each particle or particle size class must be separated and isolated out of the distribution, which results in an additional error potential. The difference between raw data points of the volume-weighted particle size distributions and the distributions fitted into individual components is expressed as a percentage and referred to as "fitting error". The fitting error is (very weakly) correlated with absolute residual error, when the design points from all bimodal mixture designs are considered ($r = 0.15$, $P \leq 0.1$). However, further correlations reinforce this as a source of error: The fitting error is moderately correlated with the individual peak overlap ($r = 0.50$, $P \leq 0.001$), and weakly correlated with the given relative volume ($r = -0.36$, $P \leq 0.001$) and the number of channels per peak ($r = -0.30$, $P \leq 0.001$) (Table 2). By manipulating these other parameters, i.e., separated and sufficient peak area, fitting error can be reduced.

Particle size measurement by static light scattering relies on the collection of a diffraction pattern from laser light that is scattered by the particles [25]. From raw scattering data, the particle size distribution is calculated by three main theories, specifically, the Frauenhofer, Mie or Rayleigh diffraction theories. Optical properties, namely, refractive indices, are required for the calculation of distributions using the Mie and Rayleigh theories [26], which must be used when particles are in the size range or smaller than the wavelength λ of the incident light. More specifically, if the particle size is smaller than six times λ, knowledge of the optical properties for particles is required [27]. Since the LS 13320 uses a λ of 750 nm, the minimum particle size for the application of the Frauenhofer scattering theory lies at 3.8 to 4.8 μm. The fermented dairy microgel particles to be analyzed in this study are in the range of 1 to 500 μm. This size range requires the particles' optical properties; however, the refractive indices of fermented dairy microgel particles are not well understood. Literature on the refractive indices of dairy proteins is limited to raw casein micelles [28] and commercially processed milk samples [29, 30], where particle properties are far removed from those present in fermented products. Furthermore, there is no research on the homogeneity of refractive indices, for example, partial surface coverings of denatured whey proteins, or regarding the influence of microgel particle responsiveness, i.e., swelling, on the particles' optical properties. In this work, real and imaginary refractive indices for the example microgel particles were set to 1.57 and 0.00, respectively. The real refractive index was estimated for the example microgel particles by following a method outlined by Hayakawa et al. [22]. However, in mixed systems, for example mixtures of standard particles and microgel particles, the refractive index is different [31]; this is not considered in the model. By selecting suitable standard particles with a refractive index similar to that of the microgel particles, or by using particles >5 μm, the influence of the refractive index is reduced (sole Fraunhofer diffraction).

Combined Factor Effects

In order to illustrate the combined effect of factors on the overall residual error as certain factors are varied, the results of the trimodal mixture designs for CA15–CA30–CA60 and CA15–CA40–CA60 are compared (Appendix: Fig. 5). With the substitution of CA30 for CA40 in the trimodal standard particle mixture design, the middle peak is shifted towards larger sizes; the size ratio relating to CA15 increases from approximately 2.2 to 3.1, and relating to CA60 decreases from 2.1 to 1.4. On the one hand, all size ratios between the three standard particles in the CA15–CA30–CA60 mixture design are greater than 2.0 and the absolute residual error for all design points is ≤5%. On the other hand, the absolute residual error for the estimated relative volume in the CA15–CA40–CA60 mixture design ranges from 0 to 15%. The span of residual error is greater for estimation of relative volume for standard particles with the smaller size ratio (CA40–CA60), ranging from −15 to +10%. Furthermore, residual error of the estimation of CA15 relative volume is greater for design points in the CA15–CA40–CA60 trimodal mixture design than in the CA15–CA30–CA60 mixture design. This is attributed to compounding factors that add to the residual error for each estimated particle relative volume, which is similarly observed for the quadmodal standard particle mixture design (Appendix: Fig. 6). For example, small or large size ratios between multiple particles lead to higher variability in the residual error for each standard particle; residual error may be even higher when a particle in the distribution is related to multiple other particles at suboptimal size ratios. The error may simply increase by this addition of factors, or interact to result in more error than anticipated.

Optimization

By consolidating and generalizing the analysis of factors contributing to residual error, certain thresholds can be defined to regulate data collection and avoid the gathering of unsuitable (high error) data. Compositional, analysis and computational factors are considered in a decision tree (Fig. 2), where the

application of the method for analyzing the volume fraction of an unknown microgel particle dispersion ϕ_{mgp} is outlined. The particle size distribution of the microgel dispersion is initially assessed, and thereafter, mixed with a suitably sized standard particle. Taking thresholds for appearance, position and size of peaks into consideration, a minimum of five acceptable particle size distributions for microgel–standard particle mixtures at different standard particle concentrations should be collected. When fitted with acceptable residual error (<5%), the distributions are used to construct a calibration curve and calculate ϕ_{mgp} (Fig. 2).

Application

Using the decision tree in Fig. 2, the ϕ_{mgp} of two example dairy microgel dispersions (process variants A and B) with and without different post-treatments were analyzed. Standard particles of known (given) volume fractions were mixed with the example microgel dispersions of unknown volume fractions but known mass fractions (and densities). By extrapolation to theoretical, proportional volume fractions of the standard particles (ratio 1:1), Eq. 6 can be used to identify the absolute volume fraction of the microgel dispersion at hand.

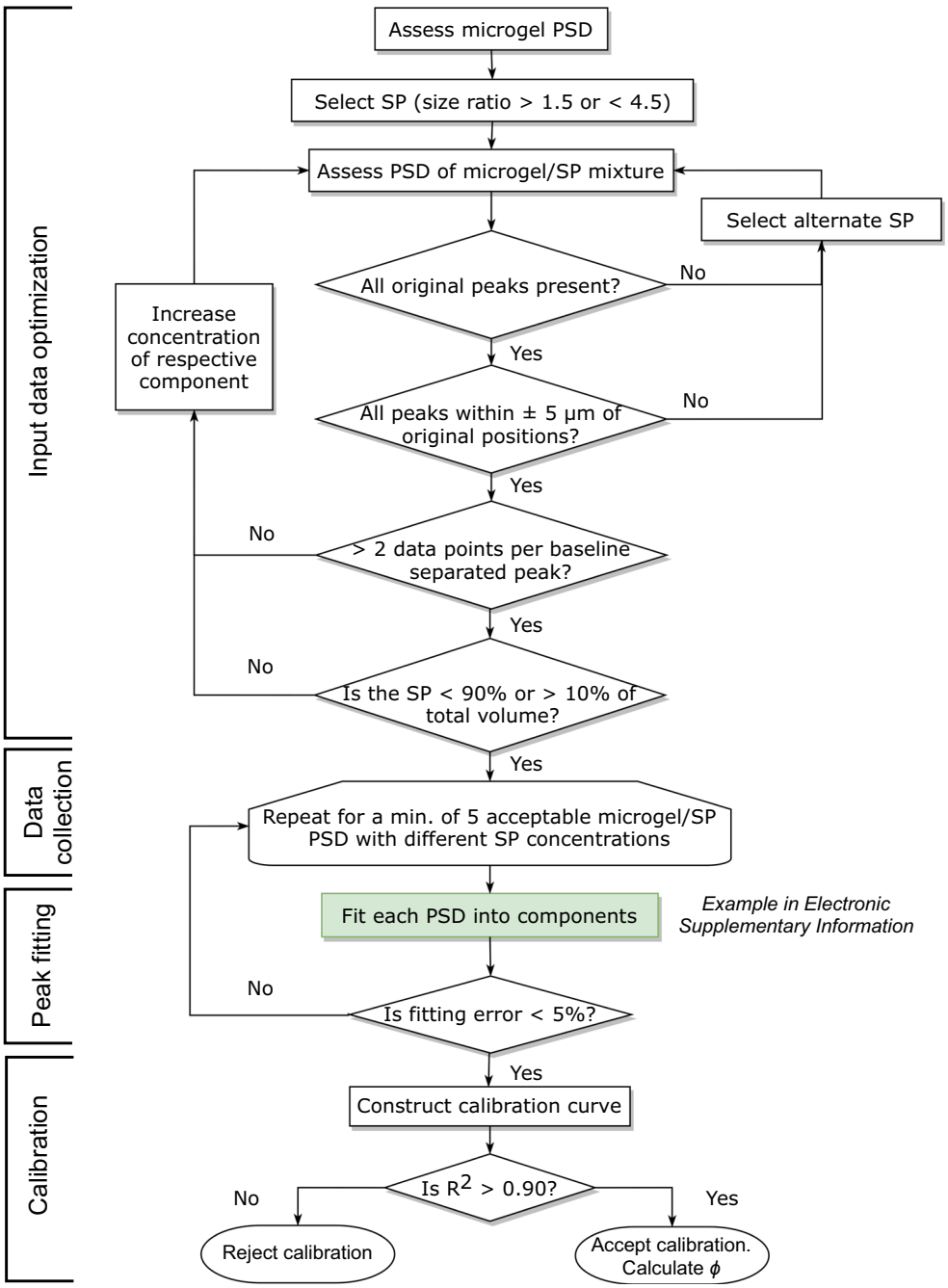

Fig. 2 Decision tree for analyzing microgel volume fraction using particle size distributions (PSD) from static light scattering and standard particle (SP) addition to ensure optimal results

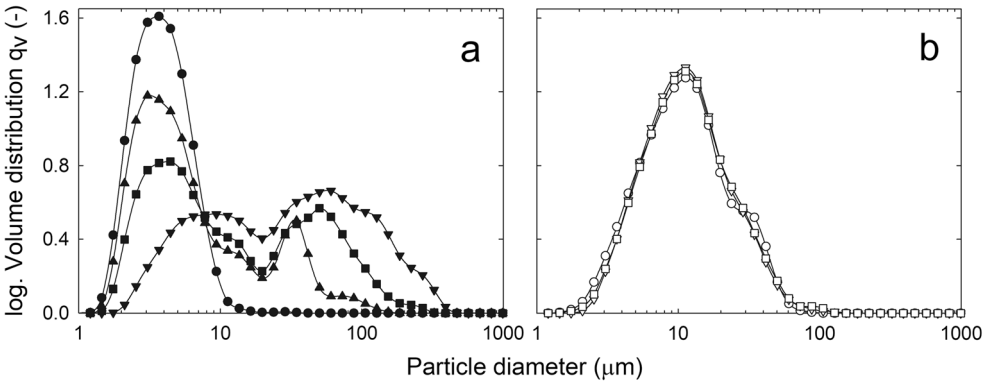

Fig. 3 Particle size distribution of microgel A (closed symbols) without post-treatment (●) or tempered for 300 min at 38 °C followed by mechanical treatment through a rotor – stator system (Ytron) with 250–255 L/h at 0 1/min (▼), 1800 1/min (■) or 4500 1/min (▲), and microgel B (open symbols) without post-treatment (○) or tempered for 300 min at 38 °C (▽) or 45 °C (□)

Particle size distributions for process variant A varied from mono- to quadmodal and ranged between 1 and 500 μm in size, depending on the post-treatment (Fig. 3a). Process variant B was bimodal and ranged between 5 and 100 μm in size for all post-treatments (Fig. 3b). The position of peaks in the particle size distributions for microgel dispersions determines the potential standard particles that can be used for the calculation of volume fraction. Since the particle size distributions for tempered process variant A samples were wide and multimodal, all process variant A samples were analyzed using two different standard particles. Due to peak locations, acceptable standard particles at acceptable size ratios, according to Fig. 2, were not found for all samples; such situations are clarified when applicable.

A summary of all average ϕ_{mgp} calculated from the respective standard particles for process variants A and B samples are listed in Table 3. Examples of calibration curves, namely, those for process variant A without post-treatment with standard particles CA15 and CA30, are provided in Fig. 4. The calculated volume fractions for process variant A (without post-treatment) using CA15 and CA30 are $\phi_{mgp} = 0.12 \pm 0.03$ and $\phi_{mgp} = 0.15 \pm 0.03$, respectively, and are not significantly different ($P > 0.05$). With increasing polydispersity and microgel particle size distribution width, due to tempering induced aggregation, [9, 11] the deviation for ϕ_{mgp} increases, exemplified by the tempered process variant A (+ 300 min, 38 °C; no mechanical post-treatment, ++ Ytron 0 1/min). In addition, ϕ_{mgp} calculated using CA15 is significantly higher than that calculated using CA30 for this sample. This is likely due to an improper choice of standard particle, i.e., size ratio between the example microgel particles and CA30, and peak superposition. The particle size distribution of the pure process variant A dispersion has a peak at approx. 30 μm (Fig. 3a), which is masked in the mixed process variant A–CA30 particle size distribution. In this case, this leads to a systematic underestimation of the volume of the example microgel particles (Table 3). The underestimation occurs, since the entire area is added to the CA30 standard particle peak and is not accounted for in the volume of the example microgel particles.

Table 3 Apparent viscosity at 10 °C, particle size and volume fraction of microgels A (9.1% *w*/w protein) and B (9.9% w/w protein) without and with post-treatments of tempering and mechanical treatment (Ytron) (i = 1, $n \geq 2$)

Microgel	Post-treatment	Viscosity	Particle size		Volume fraction ϕ_{mgp}		
		$\eta_{100\ s^{-1}}$ (Pa s) (n=2)	$d_{50,3}$ (μm) (n=6)	Span (μm) (n=6)	CA15* (n=6)	CA30* (n=6)	CA60* (n=6)
A	None (6 °C)	0.90±0.02 ^{a}	3.6±0.8 ^{a}	5.6 – 6.8	0.12±0.03 ^{a,A}	0.15±0.03 ^{a,A}	*NA*
	+ 300 min at 38 °C (=Ytron 0 1/min)	1.10±0.01 ^{a}	34.4±11.3 ^{b}	62.6 – 192.6	0.37±0.11 ^{b,A}	0.27±0.06 ^{b,B}	*NV*
	++Ytron 1800 1/min	1.11±0.01 ^{b}	8.3±2.0 ^{bc}	44.9 – 104.3	0.17±0.04 ^{a,A}	0.12±0.02 ^{a,A}	*NV*
	++Ytron 4500 1/min	1.02±0.01 ^{c}	4.5±0.7 ^{ac}	23.5 – 71.6	0.13±0.04 ^{a,A}	*NV*	0.13±0.03 ^{a,A}
B	None (6 °C)	1.52±0.07 ^{a}	11.9±1.2 ^{a}	24.0 – 35.4	*NV*	*NV*	0.40±0.10 ^{a}
	+300 min, 38 °C	1.70±0.03 ^{a}	12.2±0.8 ^{a}	21.6 – 30.7	*NV*	*NV*	0.50±0.08 ^{b}
	+300 min, 45 °C	1.96±0.12 ^{b}	12.3±0.5 ^{a}	26.5 – 29.7	*NV*	*NV*	0.54±0.07 ^{b}

Span: $d_{90.3}$ - $d_{10.3}$, range of span values given for $n = 6$

*Volume fraction calculated using the standard particle as noted

NA not analyzed; *NV* not valid

Mean values with identical superscript letters do not differ significantly (Tukey's HSD, $P < 0.05$); lowercase letters refer to differences in values in the same column (treatment); uppercase letters refer to differences in values in the same row (standard particle)

To solve this calculation problem, different (sized) standard particles can be qualified and used within the method. It should be noted that ϕ_{mgp} values calculated using CA15 and CA30 are only significantly different for process variant A tempered and without mechanical post-processing (+ 300 min, 38 °C; ++ Ytron 0 1/min) ($P < 0.05$). Furthermore, the more clearly the particle size distribution is segmented into the example microgel particles and standard particles, i.e., larger size ratios, the more accurate the calculated volume fraction is. These findings indicate good reproducibility of results using different standard particles, as well as the ability to evaluate ϕ of mono- to trimodal microgel dispersions with particle sizes between 1 and 500 μm.

Due to the bimodal nature and relatively equivalent particle sizes for the distributions of process variant B samples (Fig. 3b), it was hypothesized that the variability between calculated ϕ_{mgp} for each sample type would be lower than for multimodal process variant A samples. On the contrary, the standard deviations of ϕ_{mgp} for all process variant B samples (bimodal) are in the range of the tempered process variant A without mechanical post-processing (+ 300 min, 38 °C; ++ Ytron 0 1/min) (quadmodal), but higher than for tempered process variant A after mechanical treatment (+ 300 min, 38 °C; ++ Ytron 1800 or 4500 1/min) (trimodal). This indicates that the cause of variability is not a result of an increase in polydispersity from bi- to trimodal. Since the particle size distributions for process variant B are unchanged following tempering, the variation in ϕ_{mgp} may also stem from inherent microgel particle characteristics, which are discussed in the "Volume fraction and microgel characteristics" section. Considering the matching particle size distributions for process variant B samples, the significant difference between ϕ_{mgp} for the untempered and tempered samples should be noted. This underlines volume fraction ϕ_{mgp} as an important individual physical property to be considered, even if no difference in particle size is observable.

Volume Fraction and Microgel Characteristics

For comparison, the ϕ_{eff} is alternatively estimated using Eq. 1, on the basis of the apparent voluminosity of milk protein particles given in the literature (stirred acidified skimmed milk (micro)gels with 3.9 mL/g at 10 °C [16]; native casein micelles with 4.1 mL/g at 20 °C [14]; protein particles in pasteurized milk with 5.1 mL/g at 20 °C [15]), the density (process variant A: $\rho = 1.028$ g/mL; process variant B: $\rho = 1.013$ g/mL) and protein content (process variant A: $w = 0.091$; process variant B: $w = 0.099$). From the range of apparent voluminosities, the range of effective volume fraction for process variant A is from $\phi_{eff} = 0.36$ to 0.48 and for process variant B from $\phi_{eff} = 0.39$ to 0.51. It should be noted that these values do not consider different sample treatments, i.e., tempering and mechanical treatments.

For the tempered process variant A without mechanical post-treatment (+ 300 min, 38 °C; ++ Ytron 0 1/min), the ϕ_{mgp} of 0.37 ± 0.11 calculated with CA15 corresponds approximately to the theoretical range of ϕ_{eff}, but is relatively low for CA30 ($\phi_{mgp} = 0.27 \pm 0.06$). The higher volume fractions determined from the mixtures with CA15 appear to be the closest to the actual effective volume fraction, which corresponds to conclusions made in the "Application" section regarding CA30 as a subpar standard particle for these particle size distributions. The ϕ_{mgp} for all process variant B samples are consistent with the ϕ_{eff} range estimated from literature values. Despite the similar calculated ϕ_{eff} ranges, the ϕ_{mgp} of 0.40 ± 0.10 for process variant B without post-treatment is approximately twice as large as that for process variant A without post-treatment ($\phi_{mgp} = 0.12 \pm 0.03$ and 0.15 ± 0.03 calculated with CA15 and CA30, respectively). To account for differences in protein content between process variants A and B, one can also calculate the voluminosity for each example microgel dispersion on the basis of Eq. 1, and compare the samples based on particle volume in relation to protein. Voluminosities of $\upsilon = 1.28$ and 1.60 mL/g are calculated with CA15 and CA30, respectively, for process variant A without post-treatment. For process variant B without post-treatment, a voluminosity of $\upsilon = 3.40$ mL/g is calculated, which is approximately twice as much when compared to process variant A without post-treatment.

An additional pre-heating step (64 °C for 4.3 min) was employed in the production of process variant B after fermentation and before concentration, termed as "thermisation" in the typical production scheme for Thermoquark® (fresh cheese) [32]. Following the initial milk heat treatment at temperatures >70 °C, which results in denaturation and co-precipitation of whey proteins [33, 34], this (post-fermentation, pre-concentration) heating step increases shelf-life of fermented concentrated dairy microgel dispersions by inactivating rennet and heat-liable microorganisms [35, 36]. Further heating of milk at temperatures >80 °C results in fermented dairy microgel dispersions with increased yield and a smoother texture, caused by higher serum binding of the denatured whey proteins [34, 37, 38]; conversely, literature regarding the effect of a (post-fermentation, pre-concentration) heating step on particle size and rheological characteristics remains to be found. Comparing process variants A and B in this study, it is postulated that (post-fermentation, pre-concentration) heating causes rearrangements in the protein particles that lead to higher levels of bound serum. Thus, the individual microgel particles have higher volumes and further aggregation is inhibited.

As demonstrated by the differences between ϕ_{mgp} for process variants A and B, with and without post-treatments of tempering and mechanical input, this method provides an opportunity to compare and evaluate samples of the same composition and different treatments that affect the voluminosity, i.e., temperature, time, shear stress, and shear rate. The results of the ϕ_{mgp} analysis confirm that these factors affect volume fraction and provide the

first possible values for the volume fraction of environmentally responsive and mechanically sensitive microgel dispersions.

Along with significant changes in ϕ_{mgp}, the viscosity and particle size parameters are also affected. With increasing energy input, or rotational speed of the rotor–stator device, the ϕ_{mgp} decreases to below 25%, accompanied by a decrease in the mean particle size and apparent viscosity (process variant A, Table 3). For apparent viscosity and particle size parameters, the increases upon tempering and decreases upon subsequent mechanical treatment are in line with previous findings regarding post-processing of fresh cheese [9, 11]. Upon tempering, the increase in particle size is attributed to rearrangement and dense clustering of aggregated particles [11, 39, 40]. At higher temperatures, the strength and number of hydrophobic bonds within the fermented dairy microgel particles increases [41], causing particle shrinkage, as well as increased deformability. Thus, an assumption of decreased particle volume ensues. The decrease in apparent viscosity is attributed to a release of entrapped serum from the fermented dairy microgel particles, because of a loss of gel structure [12], which has previously been substantiated by evaluation of forced syneresis [11]. However, it could be shown for the first time that the increase and successive decrease in apparent viscosity is not exclusively due to the aggregation and breakdown of the fermented dairy microgel particles (particle size) and serum release in general [11], but to a lower volume of each particle after mechanical treatment.

Though process variants A and B were both tempered during post-treatments, the increases in ϕ_{mgp} and apparent viscosity are accompanied by an increase in particle size only for process variant A and not process variant B (Table 3). This is attributed to the different production methods used for process variants A and B, where process variant B was produced with an additional (post-fermentation, pre-concentration) heating step. Since this heating step increased the volume fraction, this indicates that the fermented dairy microgel particles were still able to increase in volume, regardless of a hindered ability to aggregate. Though the ϕ_{mgp} is significantly higher for process variant B tempered at 38 and 45 °C than the process variant B without post-treatment, standard deviations are high compared to process variant A, in spite of low polydispersity. In the previous section, it was noted that polydispersity does not account for the higher standard deviations for ϕ_{mgp} of process variant B. The uniformity and ability of the fermented dairy microgel particles to bind higher amounts of serum when tempered is likely the source of this observation.

Conclusion

A new method to characterize soft particle volume has been developed and applied to an example environmentally responsive microgel dispersion. The approach enables the quantification of particle volume and volume fraction for soft microgel particles, in relation to absolute (given) standard particle volume fractions. Quantification of soft particle volume fraction allows one to interpret rheological and textural data in the context of the (altered) volume fraction for the first time, and to apply basic rheological principles of (multimodal) mixtures. Furthermore, volume-weighted particle size distributions are commonly measured by static light scattering when investigating structure – function relationships. Thus, adapting this method of analysis to include determination of volume fraction is an effective way to optimize equipment and time usage. In addition, it is easy to adapt to other types of microgel dispersions and deals with in-sample variance due to inhomogeneity and non-spherical particles.

The determination of the volume fraction of soft (microgel) particle dispersions based on relative volumes, in relation to qualified standard particles, could be applied robustly within a wide range of particle sizes (1 to 500 μm) and multimodal size distributions (up to quadmodal). Moreover, the sample size and time requirements can be reduced (approximately 45 min per calibration curve) by skillfully selecting the size of standard particles and the levels of the mixing ratios/given relative volumes. Apart from proper selection of the standard particles, method sensitivity can be improved by optimizing the spatial resolution of the laser diffraction system and determining the apparent refractive index of the soft matter in question. Additionally,

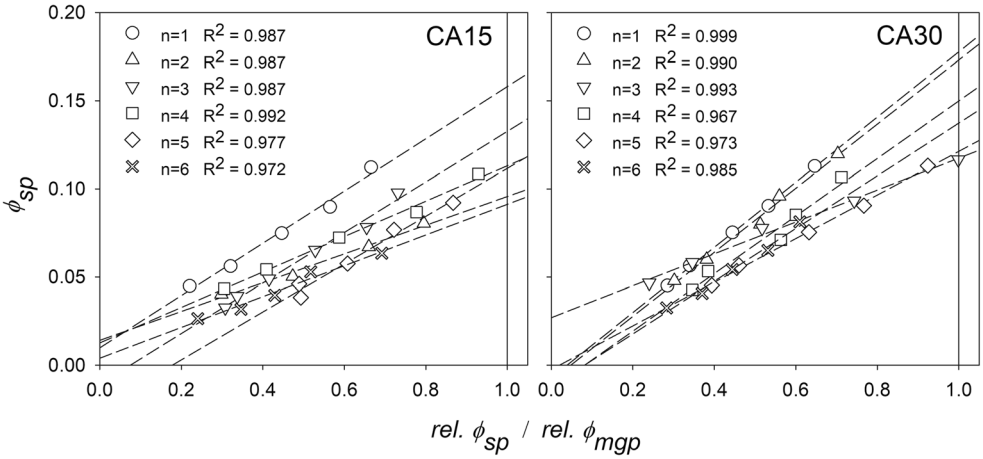

Fig. 4 Calibration curves for microgel A (without post-treatment) using CA15 (left) and CA30 (right) as standard particles ($n = 6$ independent measurements); unknown microgel volume fraction is taken from extrapolation to the known volume fraction of the standard particles: $\phi_{calc} = \phi_{sp} = \lim_{ratio \to 1:1} rel.\phi_{sp}/rel.\phi_{mgp}$

environmental parameters, such as pH, ionic strength, and osmotic pressure, can be adjusted by modifying the medium employed for dilution and particle size measurements, in order to determine the relationships with microgel particle voluminosity. Due to its simplicity and a broad range of accessible particle sizes, we expect this approach to be applicable to a wide range of soft materials.

Supplementary Information The online version contains supplementary material available at https://doi.org/10.1007/s11483-021-09665-z.

Acknowledgements This IGF Project of the FEI was supported via AiF within the programme for promoting the Industrial Collective Research (IGF) of the German Ministry of Economic Affairs and Energy (BMWi), based on a resolution of the German Parliament. Project AiF 19012 N. Financial support was also provided by the Natural Sciences and Engineering Research Council of Canada (NSERC) in the form of a doctoral scholarship. The authors thank Stephan Bücker for performing parts of the particle size measurements, as well as Luc Mertz and Nabil Chaib for assistance with fresh cheese production.

Authors' Contributions All authors contributed to the study conception and design. Material preparation, data collection and analysis were performed by Anisa Heck. The first draft of the manuscript was written by Anisa Heck and all authors commented on previous versions of the manuscript. All authors read and approved the final manuscript.

Funding Open Access funding enabled and organized by Projekt DEAL. This IGF Project of the FEI was supported via AiF within the programme for promoting the Industrial Collective Research (IGF) of the German Ministry of Economic Affairs and Energy (BMWi), based on a resolution of the German Parliament. Project AiF 19012 N.

Compliance with Ethical Standards

Conflict of Interest The authors declare that they have no conflict of interest.

Appendix

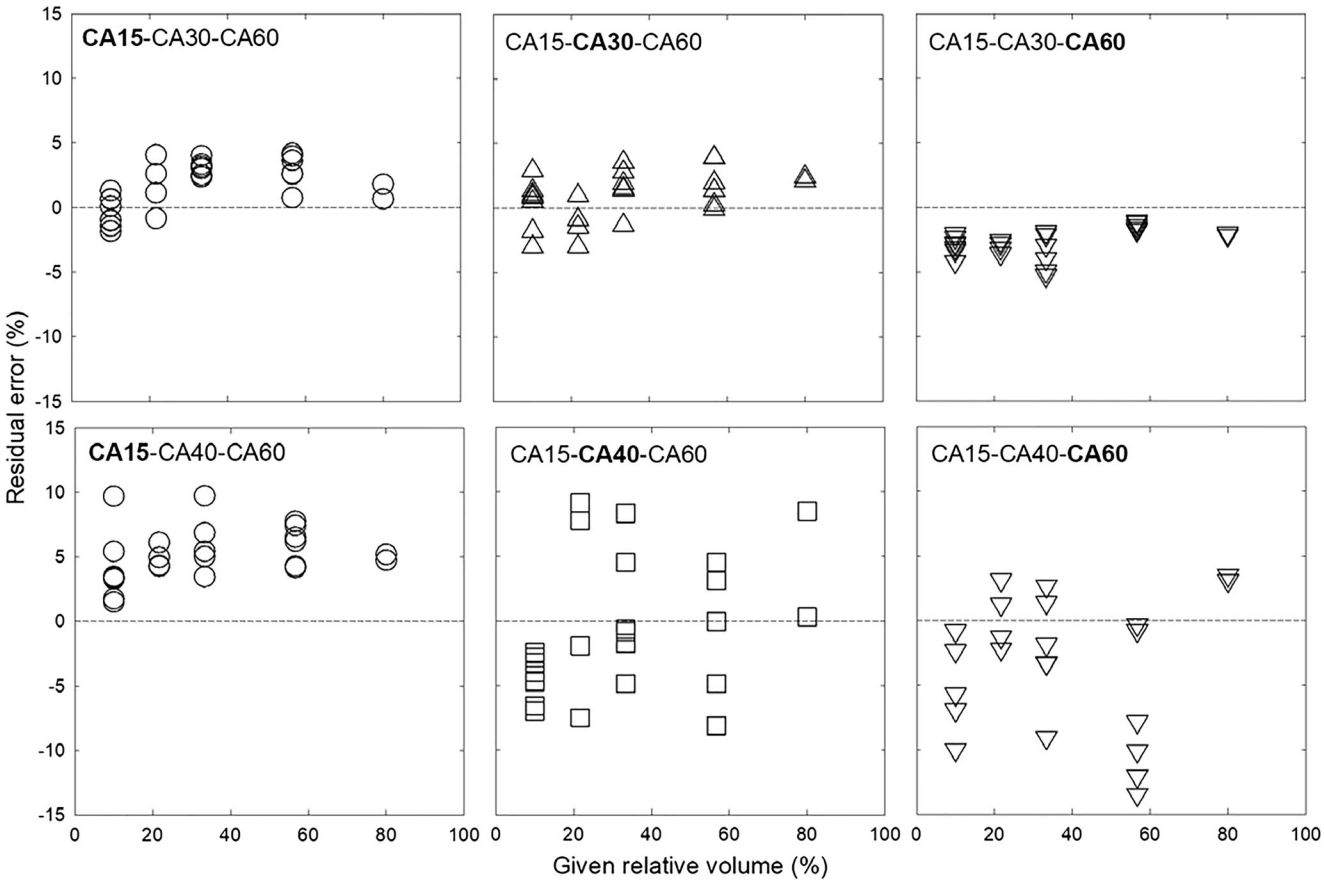

Fig. 5 Residual error of the fitted particle size distributions in relation to sample composition of trimodal standard particle mixtures (top row CA15-CA30-CA60; bottom row CA15-CA40-CA60; depicted standard particle listed in bold) in terms of standard particle relative volume (CA15 ○; CA30 Δ; CA40 □; CA60 ▽); residual error is defined as over or under assessment of particle volume in comparison to sample composition (given relative particle volume); dotted line indicates 0% error

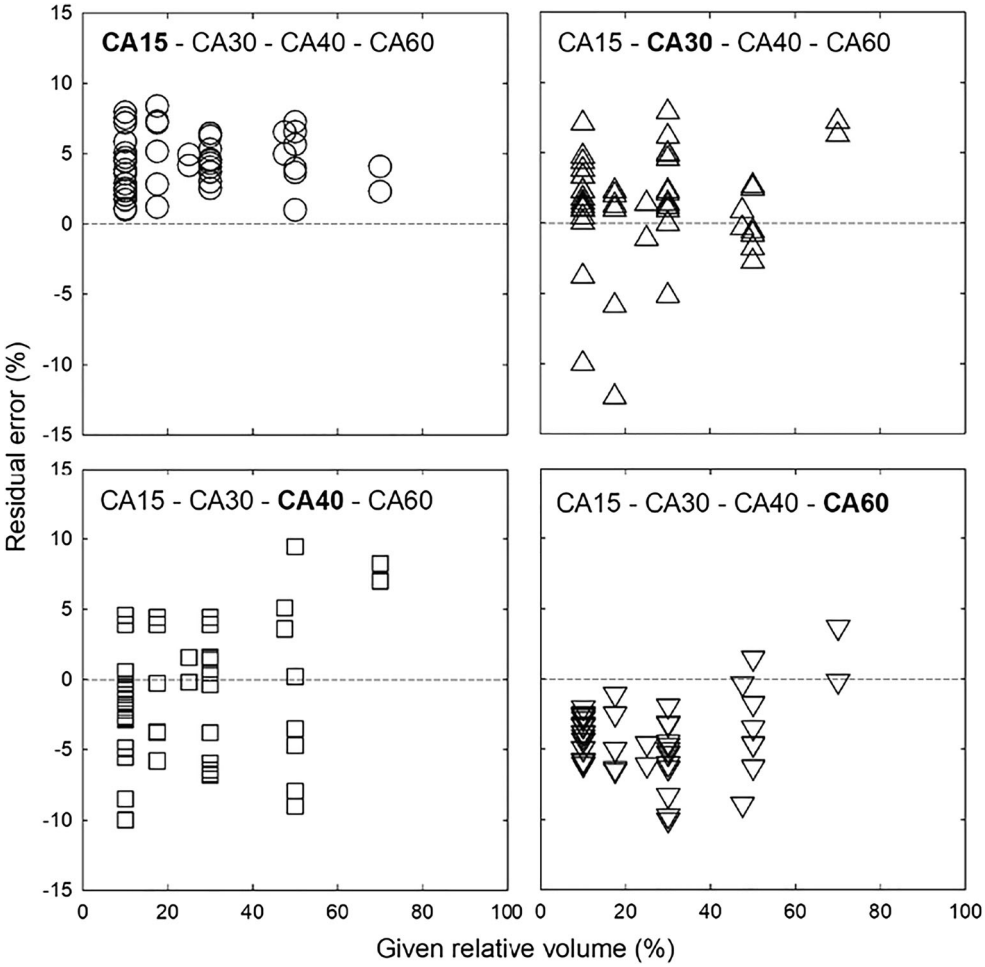

Fig. 6 Error of the fitted particle size distributions in relation to sample composition of quadmodal standard particle mixture in terms of standard particle relative volume (CA15 ○; CA30 Δ; CA40 □; CA60 ▽); composition and error displayed in relative volume % where the overall composition is equal to 100% and error is defined as over or under assessment of particle volume in comparison to sample composition (given relative particle volume); dotted line indicates 0% error

Table 4 Final regression analysis after backwards stepwise selection for the relationship between sample composition (given relative particle volume) and residual error expressed in percent for the first listed particle in bimodal mixtures of spherical PMMA particles analyzed by static light scattering

Mixture	Model fit			*P* - values[a]				Regression coefficients[a]				
	SER[b]	Lack of fit[c]	R^2 adj	Linear[d]	Quadratic	Inverse 1	Inverse 2	Linear 1[d]	Linear 2[d]	Quadratic	Inverse 1	Inverse 2
CA15-CA30	**0.5**	**0.521**	0.901	<0.001	–[e]	–	–	−4.1	1.1	–[e]	–	–
CA15-CA40	**0.7**	**0.078**	0.281	0.030	–	–	–	2.8	4.7	–	–	–
CA15-CA60	**1.1**	0.006	0.459	0.226	0.039	0.049	0.081	−21.4	−26.4	87.5	1.8	1.5
CA30-CA40	4.2	**0.421**	0.507	0.013	–	0.008	0.008	−26.1	19.6	–	−2.8	2.9
CA30-CA60	**1.0**	**0.704**	0.326	0.453	–	0.046	–	2.8	4.1	–	−0.3	–
CA40-CA60	**1.5**	**0.604**	0.914	0.247	0.002	–	0.001	−20.9	−14.5	57.1	–	2.5

Regression equation $\widehat{y} = x_1 + x_2 + x_1\,x_2 + 1/x_1 + 1/x_2$

where X_1 and X_2 are defined as the first (1) and second (2) particles listed in each bimodal mixture

[a] Regression coefficients and *P* values for the second (2) particle (not shown) are identical, with regression coefficients having opposite signs (+, −)

[b] SER Standard error of the estimate values in **bold** show models where residual error values lie within ≤1.5 of the fitted regression line

[c] Lack of fit values in **bold** show models that adequately describe the data

[d] Linear terms are mandatory in regression analysis of mixture designs since any change in a factor must impact the other factors

[e] Absence of a *P* value or regression coefficient indicates this term was omitted during backward stepwise analysis based on $p \geq 0.10$

Open Access This article is licensed under a Creative Commons Attribution 4.0 International License, which permits use, sharing, adaptation, distribution and reproduction in any medium or format, as long as you give appropriate credit to the original author(s) and the source, provide a link to the Creative Commons licence, and indicate if changes were made. The images or other third party material in this article are included in the article's Creative Commons licence, unless indicated otherwise in a credit line to the material. If material is not included in the article's Creative Commons licence and your intended use is not permitted by statutory regulation or exceeds the permitted use, you will need to obtain permission directly from the copyright holder. To view a copy of this licence, visit http://creativecommons.org/licenses/by/4.0/.

References

1. H.M. Shewan, J.R. Stokes, J. Colloid Interface Sci. **442**, 75–81 (2015)
2. A. Loewen, S. Nöbel, and J. Hinrichs, in *Ref. Modul. Food Sci*. (Elsevier, 2017), pp. 1–9
3. W.C.K. Poon, E.R. Weeks, C.P. Royall, Soft Matter **8**(1), 21–30 (2012)
4. S. Adams, W.J. Frith, J.R. Stokes, J. Rheol. (N. Y. N. Y) **48**, 1195 (2004)
5. D. Vlassopoulos, M. Cloitre, Curr. Opin. Colloid Interface Sci. **19**(6), 561–574 (2014)
6. S.H. Ching, N. Bansal, B. Bhandari, Food Res. Int. **80**, 50–60 (2016)
7. Z.L. Yao, N. Grishkewich, K.C. Tam, Soft Matter **9**(22), 5319 (2013)
8. I. Fernández Farrés, R.J.A. Moakes, I.T. Norton, Food Hydrocoll. **42**, 362–372 (2014)
9. C. Hahn, M. Sramek, S. Nöbel, J. Hinrichs, Dairy Sci. Technol. **92**(1), 91–107 (2012)
10. A. Körzendörfer, S. Nöbel, J. Hinrichs, Food Res. Int. **97**, 170–177 (2017)
11. C. Hahn, T. Wachter, S. Nöbel, J. Weiss, H. Eibel, J. Hinrichs, Int. Dairy J. **26**(1), 73–77 (2012)
12. A. Mokoonlall, S. Nöbel, J. Hinrichs, Trends Food Sci. Technol. **54**, 26–36 (2016)
13. B. Dames, B.R. Morrison, N. Willenbacher, Rheol. Acta **40**(5), 434–440 (2001)
14. S. Nöbel, K. Weidendorfer, J. Hinrichs, J. Colloid Interface Sci. **386**(1), 174–180 (2012)
15. M.E. van Marle, D. van den Ende, C.G. de Kruif, J. Mellema, J. Rheol. (N. Y. N. Y) **43**, 1643 (1999)
16. L. G. B. Bremer, Fractal Aggregation in Relation to Formation and Properties of Particle Gels, Wageningen Agricultural University (1992)
17. H.M. Shewan, J.R. Stokes, J. Nonnewton. Fluid Mech. **222**, 72 (2014)
18. D. Quemada, **94**, 82 (1977)
19. S. H. Maron and P. E. Pierce, **11**, 80 (1956)
20. R. S. Farr and R. D. Groot, 1 (2009)
21. N. Willenbacher, J.S. Vesaratchanon, O. Thorwarth, E. Bartsch, Soft Matter **7**(12), 5777 (2011)
22. O. Hayakawa, K. Nakahira, J.I. Tsubaki, Adv. Powder Technol. **6**(1), 47–61 (1995)
23. C. Hahn, S. Nöbel, R. Maisch, W. Rösingh, J. Weiss, J. Hinrichs, Food Hydrocoll. **49**, 183–191 (2015)
24. Beckman Coulter, *LS 13 320 Particle Size Analyzer Manual* (2011)
25. O. Glatter, in *Scatt. Methods Their Appl. Colloid Interface Sci.*, edited by O. B. T.-S. M. and their A. in C. and I. S. Glatter (Elsevier, 2018), pp. 175–185
26. O. Glatter, in *Scatt. Methods Their Appl. Colloid Interface Sci.*, edited by O. B. T.-S. M. and their A. in C. and I. S. Glatter (Elsevier, 2018), pp. 265–297
27. G. Mie, Ann. Phys. Berlin **25**, 377 (1908)
28. S. Stocker, F. Foschum, P. Krauter, F. Bergmann, A. Hohmann, C. Scalfi Happ, A. Kienle, Appl. Spectrosc. **71**(5), 951–962 (2017)
29. W.R. Calhoun, H. Maeta, S. Roy, L.M. Bali, S. Bali, J. Dairy Sci. **93**(8), 3497–3504 (2010)
30. A.J. Jääskeläinen, K.-E. Peiponen, J.A. Räty, J. Dairy Sci. **84**(1), 38–43 (2001)
31. H. Choi, W. Lee, S. Kim, W.-S. Jung, J.-H. Kim, Mater. Chem. Phys. **117**(1), 18–22 (2009)
32. D. Schulz-Collins and B. Senge, *in Cheese - Chem. Phys. Microbiol*. (3rd ed (2004)), pp. 301–328
33. P.M. Kelly, B.T. O'Kennedy, Int. Dairy J. **11**(4-7), 525–532 (2001)
34. J. Hinrichs, Int. Dairy J. **11**(4-7), 495–503 (2001)
35. N. Y. Farkye, *Quark, Quark-like Products, and Concentrated Yogurts* (Elsevier, 2017)
36. E. Zakrzewski, L. Stepaniak, R.K. Abrahamsen, T. Sørhaug, Int. Dairy J. **1**(3), 199–208 (1991)
37. J.A. Lucey, C.T. Teo, P.A. Munro, H. Singh, J. Dairy Res **64**, 591 (1997)
38. M. Vaziri, H. Abbasu, A. Mortazavi, H. Abbasi, A. Mortazavi, J. Food Process. Preserv. **34**, 2–14 (2010)
39. W.J. Lee, J.A. Lucey, J. Dairy Sci. **87**(10), 3153–3164 (2004)
40. J.A. Lucey, T. van Vliet, K. Grolle, T. Geurts, P. Walstra, Int. Dairy J. **7**(6-7), 381–388 (1997)
41. S. P. F. M. Roefs and T. van Vliet, **50**, 161 (1990)

Publisher's Note Springer Nature remains neutral with regard to jurisdictional claims in published maps and institutional affiliations.